American Mineralogist, Volume 82, pages 182–193, 1997

Gold-bearing arsenian pyrite and marcasite and arsenopyrite from Carlin Trend gold deposits and laboratory synthesis

MICHAEL E. FLEET[1] AND A. HAMID MUMIN[2]

[1]Department of Earth Sciences, University of Western Ontario, London, Ontario, Canada N6A 5B7
[2]Department of Geology, Brandon University, Brandon, Manitoba, Canada R7A 6A9

ABSTRACT

Invisible gold in natural and synthetic arsenian pyrite and marcasite correlates with anomalous As content and Fe deficiency, and high contents of invisible gold in most natural and all synthetic arsenopyrite correlate with excess As and Fe deficiency. As-rich, Fe-deficient arsenopyrite synthesized hydrothermally contains up to 3.0 wt% Au uniformly distributed in growth zones of light backscattered electron contrast. At the Deep Star gold deposit, Carlin Trend, Nevada, the sulfide compositions apparently span the full range of metastability from FeS_2 to near FeAsS (40 at% S); arsenian pyrite contains up to 0.37 wt% Au, but arsenopyrite has excess S and is relatively Au poor. Observed minimum Fe contents are 29.1 at% in arsenian pyrite and marcasite from the Deep Star deposit and 31.3 at% in synthetic arsenopyrite. We suggest that invisible gold in arsenian pyrite and marcasite and arsenopyrite from sediment-hosted gold deposits represents Au removed from ore fluids by chemisorption at As-rich, Fe-deficient surface sites and incorporated into the solids in metastable solid solution. However, the oxidation state of invisible gold (Au^0, Au^{1+}) remains uncertain because the chemisorption process is intrinsically nonsystematic in terms of crystal-chemical parameters and does not result in definitive atomic substitution trends.

INTRODUCTION

In sediment-hosted gold deposits and some mesothermal lode-gold deposits, a substantial fraction of Au is present as "invisible gold" within grains of iron sulfide and sulfarsenide minerals (principally pyrite and arsenopyrite). Previous studies have established that invisible gold is spatially associated with local As enrichment in pyrite grains (Wells and Mullens 1973; Fleet et al. 1989; Cook and Chryssoulis 1990; Bakken et al. 1991; Fleet et al. 1993; Arehart et al. 1993; Mumin et al. 1994; Michel et al. 1994). Fleet et al. (1993) concluded that Au is probably incorporated into metastable solid solution in arsenian pyrite via As-rich growth surfaces. Similarly, Arehart et al. (1993) suggested that Au in arsenian pyrite is present as a charged species (Au^{3+}) and was probably deposited with As as coupled substitutions in pyrite. However, the chemical state of invisible gold in pyrite remains controversial because (1) the substitution reaction(s) has not been demonstrated through element correlations, (2) submicroscopic particles of Au (colloidal gold) may be present (e.g., Bakken et al. 1989; Cook and Chryssoulis 1990; Mao 1991; Fleet et al. 1993), and (3) available spectroscopic techniques yield ambiguous results for trace amounts of Au (e.g., Mössbauer spectroscopy: Cathelineau et al. 1989; Wagner et al. 1994; X-ray photoelectron spectroscopy (XPS): Mycroft et al. 1995).

Fleet et al. (1989, 1993) and MacLean (1991) developed a potassium permanganate staining technique for polished sections of ore minerals and used it to map the As distribution in pyrite grains from a wide variety of gold deposits. The resulting complex optical micrographs revealed both multistage and episodic rock-fluid activity in in situ gold-deposit systems. An early application of their surface-staining procedure showed that the compact rounded pyrite grains in quartz-pebble conglomerate gold ore from the Witwatersrand basin of South Africa were indeed detrital in origin (MacLean and Fleet 1989), thus providing further evidence for a detrital origin for this important class of gold deposit. From Fleet et al. (1989, 1993), MacLean (1991), Mumin et al. (1994), and unpublished work, authigenic arsenian pyrite appears to be associated with sediment-hosted, epithermal, and low-temperature mesothermal gold deposits in carbonate-bearing host rocks that have not been metamorphosed beyond middle low-grade conditions.

Fleet et al. (1989) reported As contents in pyrite from gold deposits of up to 8 wt% (5 at%), far in excess of the maximum As content expected from laboratory experiments in the dry Fe-As-S system (Clark 1960) extrapolated to low and very-low geological temperatures. They demonstrated an inverse correlation of As with S consistent with the solid solution $Fe(S_{1-x}As_x)_2$ for the natural arsenian pyrite of their study. However, the compositions of natural and synthetic arsenopyrite (FeAsS) have been interpreted as indicating both a ligand and a cation role for As (e.g., Johan et al. 1989; Wu and Delbove

0003–004X/97/0102–0182$05.00

1989). For arsenopyrite from the Central Massif, France, Johan et al. (1989) reported enrichment in Au and Sb of up to 1.5 and 1.6 wt%, respectively, and a marked deficiency of Fe, which was interpreted to represent the complex solid solution $(Fe,Au,As,Sb)As_{1\pm x}S_{1\pm x}$ and a substitution mechanism of 2As = Au (or Sb) + Fe. In apparent contrast, Wu and Delbove (1989) synthesized compositionally zoned arsenopyrite with up to 1.7 wt% Au in the system Fe-As-S-O-NaCl(KCl)-H_2O at 500 °C and 2 kbar, and reported a substitution mechanism of Fe = Au. More generally, the role of As and the mechanisms of valence compensation in pyrite-marcasite-arsenopyrite group compounds remain mysterious (e.g., Tossel et al. 1981; Wijeyesekera and Hoffmann 1983). Kuranti (1941) is credited with documenting solid solution of Au in synthetic pyrite from chemical analysis and unit-cell spacing, but no details are available and his experiments have not been repeated with modern analytical procedures.

We presently report on Au-bearing arsenian pyrite and marcasite and arsenopyrite from Carlin Trend deposits, Nevada, and from laboratory synthesis. The study further documents the extraordinary control of surface chemistry on the uptake of Au and As by these minerals and the crystallization of metastable solid solutions. However, the precise oxidation state of the Au incorporated into these sulfides and sulfarsenides (Au^0, Au^{1+}) remains uncertain.

Iron sulfides and sulfarsenides from Carlin Trend deposits

The prominent ranking of the United States in world gold production is due mostly to output from the sediment-hosted (Carlin-type) deposits of Nevada. The geology and origin of these important gold deposits were reviewed recently by Berger and Bagby (1991) and Christensen (1993). The gold deposits are both passive replacements and hydrothermal and tectonic breccias and occur predominately in Paleozoic and early Mesozoic marine sedimentary and volcanic rocks, and particularly in carbonaceous, finely laminated silty carbonates, which are commonly dolomitic, and carbonate-bearing siltstones. There is often a close spatial association with granodioritic or alkaline igneous intrusions of Jurassic-Cretaceous age. The unusual and characteristic ore mineralogy of invisible gold in As-rich rims of pyrite grains has been extensively studied (e.g., Wells and Mullens 1973; Radtke 1985; Bakken et al. 1991; Arehart et al. 1993). Bakken et al. (1991) used secondary ion mass spectrometry (SIMS) to show that Au was associated with As- and Sb-bearing rims of auriferous pyrite from the Post deposit. Colloidal gold particles were not identified at 20–50 Å resolution in their parallel transmission electron microscopy (TEM) study. Arehart et al. (1993) studied samples from the Chimney Creek, Gold Acres, Gold Quarry, Post-Betze, and Rain deposits, using scanning electron microscopy (SEM) and SIMS. They reported that the Au was associated largely with arsenian pyrite present as rims on, and narrow veinlets in, Au-free pyrite.

The Carlin Trend follows the line of the Tuscarora Mountains, Nevada, and includes several very large gold deposits (Post-Betze, Genesis, Gold Quarry, Carlin) and numerous smaller ones, including the Deep Star deposit. The gold deposits in the Deep Star–Genesis–Post-Betze area are spatially associated with the Goldstrike intrusion, a composite dioritic to granodioritic stock of Cretaceous age (about 150 m.y.), which has locally metamorphosed the overturned middle Paleozoic strata to hornfels and marble with extensive exo- and endoskarns. The ore mineralogy consists of pyrite, arsenian pyrite, arsenian marcasite, arsenopyrite, realgar, and orpiment. The age of mineralization has been constrained to the period between 120 to 35 m.y., although there remains considerable controversy on the precise timing in individual deposits (Christensen 1993; Rota 1993). Higher level and lower temperature ores are disseminated and clearly replacement type in nature, and are located where permeable stratigraphic units provided channelways for mineralizing fluids. The ore mineralogy is very-fine-grained pyrite and marcasite. With increasing depth in the ore system or proximity to structural feeder zones, changes in both ore textures and mineralogy suggest progressively increasing temperatures of deposition. Deeper level and higher temperature ores are largely structurally controlled and associated with fault breccias. The ore mineralization is of larger grain size and consists of pyrite, marcasite, and increasingly abundant arsenopyrite. At the Gold Quarry and Genesis deposits the fault breccias associated with the deeper level ores evidently represent structural feeder zones for the higher level replacement ores. Supergene oxidation of sulfides along the Carlin Trend extends to variable depths of up to 300 m.

The Deep Star deposit, from which most of the present samples were obtained, consists of deeper level, fault-breccia-related ore only. The deposit is hosted within exo- and endoskarns of the contact metamorphic aureole associated with the Goldstrike intrusion. Host rocks for the mineralization include calc-silicate hornfels and marble of the Popovich Formation, and strongly altered portions of the intrusion. Alteration and ore minerals include quartz, sericite, dolomite, kaolinite, montmorillonite, pyrite, marcasite, arsenopyrite, realgar, orpiment, and trace amounts of other sulfides. The Au:Ag ratio is high (up to 50:1), and the Au grade increases with the presence and abundance of very-fine-grained quartz-kaolinite alteration and high pyrite-marcasite content. Abundant ultra-fine-grained pyrite and marcasite give ore rocks a sooty appearance, which can be mistaken for graphite.

Samples of gold sulfide ore from the Deep Star, Gold Quarry, Genesis, and Carlin deposits were obtained during a visit to the Newmont Gold Mining operations at Carlin, Nevada, in December 1994. Polished thin sections typical of unoxidized moderate- and high-grade fault-breccia ore from drill holes DS-3, DS-9, DS-63 (Deep Star deposit), BSN-389 (North Star deposit), CAT-699 (West Genesis deposit), QRC-644 and QRC-1322 (Gold Quarry deposit), and hand samples from the Genesis open pit were investigated. Polished thin sections typical of

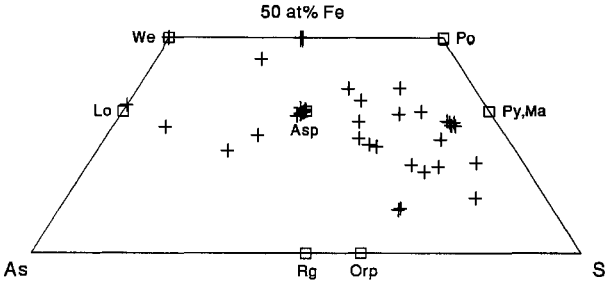

FIGURE 1. Bulk Fe-As-S compositions investigated in hydrothermal experiments at 205–605 °C, 1.3–1.6 kbar (plus signs). Open squares are ideal compositions of westerveldite (We), pyrrhotite/troilite (Po), löllingite (Lo), arsenopyrite (Asp), pyrite (Py), marcasite (Ma), realgar (Rg), and orpiment (Orp).

unoxidized moderate- and high-grade disseminated ore from underground workings immediately beneath the open pit at the Carlin deposit and from the Gold Quarry open pit were also investigated. The ore samples were studied by ore microscopy, potassium permanganate staining, and electron microprobe analysis (EMPA; below).

EXPERIMENTAL METHODS

Ore minerals in the system Fe-As-S-Au were synthesized hydrothermally using standard Tuttle cold-seal bombs and gold capsules. Charges consisted of 0.03–0.08 g of Fe-As-S, prepared variously from FeAs, FeS, a commercial synthetic pyrite (FeS_2), natural arsenopyrite, As, S, and an As-S composition with about 60 at% As (AS1), 0.02 g NaCl (or KCl, $CaCO_3$), and 0.01 g H_2O (Fig. 1; Table 1). Synthetic starting materials were prepared from high-purity elements, salts were ACS certified, and H_2O was deionized. Starting materials were generally granular; they were not ground and mixed, but some mixing did occur during loading of the charges. Gold capsules were of fine gold and were the source of Au in the experimental system. The experimental conditions varied from 205 to 605 °C, 1.3 to 1.6 kbar, and 3 to 57 day run times. In general, löllingite and westerveldite were investigated at 500–600 °C, arsenopyrite at 300–600 °C, arsenian pyrite and marcasite at 300–500 °C, and FeS_2-AsS-S–composition material at 200–300 °C. All experiments were quenched in water. Chloride salts were removed by washing in warm water, and the residue was dried in air at 105 °C for 1–2 h. The sulfide products were investigated by ore microscopy, potassium permanganate staining, EMPA, and X-ray diffraction.

Fe, S, As, and Au were determined in situ for both natural and synthetic ore minerals of this study by EMPA, using a JEOL JXA 8600 Superprobe operated at 20 kV and 20 nA, a beam diameter of 2 μm, the Au$L\alpha$ line, and 50 s counts on peak and background for Au. Selected spot analyses were repeated at 25 kV and 35 nA with no significant change in the results. Natural pyrite was used to calibrate Fe and S in pyrite, arsenian pyrite, marcasite, and pyrrhotite, and arsenopyrite was used for Fe and S

TABLE 1. Representative EMPA compositions for phases in the Fe-As-S-Au system

Phase	We	Po	Po	Lo	Apy	Apy	Ma	Ma	Py	Py	Py	Py
Expt.	SA20	SA22	SA27	SA21	SA18	SA43	SA7	SA7	SA3	SA3	SA3	SA9
						wt%						
Fe	43.8	63.0	60.4	27.4	30.4	35.2	42.0	38.9	43.5	44.8	44.0	43.0
As	57.2	0.1	0.0	70.4	53.5	24.2	10.5	12.6	7.0	2.9	6.2	7.7
S	0.0	37.1	39.4	2.0	14.7	39.9	48.9	49.4	49.6	53.0	49.6	48.6
Au	0.0	0.06	0.03	0.19	0.87	0.14	0.0	0.35	0.08	0.06	0.06	0.37
Total	101.0	100.2	99.9	100.0	99.5	99.4	101.3	101.2	100.1	100.7	99.8	99.7
						at%						
Fe	50.7	49.4	46.8	32.8	31.6	32.7	31.1	29.0	32.2	32.2	32.5	32.2
As	49.3	0.0	0.0	62.9	41.5	27.7	5.8	7.0	3.9	1.5	3.4	4.3
S	0.0	50.6	53.2	4.2	26.6	39.2	63.1	64.0	64.0	66.3	63.8	63.4
Au	0.0	0.01	0.01	0.06	0.26	0.04	0.0	0.07	0.02	0.01	0.01	0.08
						Starting composition (at%; materials)						
Fe	34.8	50.0	33.1	29.7	32.7	30.8	29.8		21.0			31.0
As	65.2	26.0	12.5	60.6	34.5	24.9	7.9		8.5			8.8
S	0.0	24.0	54.4	9.7	32.7	44.3	62.3		70.6			60.3
FeAs	X	X	X	X								
FeS		X			X	X	X					X
Py			X			X			X			
As	X			X	X	X						
S			X	X			X		X			X
As1							X		X			X
						Experimental conditions						
T (°C)	505	505	605	505	414	400	310		310			405
P (kbar)	1.6	1.6	1.6	1.6	1.5	1.5	1.4		1.4			1.5
salt	NaCl	NaCl	NaCl	NaCl	NaCl	NaCl	NaCl		NaCl			KCl
t (d)	6	6	5	6	14	57	20		20			7

Note: As1 is $As_{60}S_{40}$; We = westerveldite, Po = pyrrhotite, Lo = löllingite, Apy = arsenopyrite, Ma = marcasite, Py = pyrite, X = starting material.

in analyses of arsenopyrite, löllingite, and westerveldite. The arsenopyrite standard was used for As, and pure gold for Au. We found that our sample of Asp57 of Kretschmar and Scott (1976) exhibited too much spatial variation in composition for use as a standard, but our sample of Asp200 was surprisingly homogeneous and was therefore adopted as the arsenopyrite standard. Back analysis of this standard over 16 separate EMPA sessions resulted in an average Fe content of 34.53 ± 0.18 wt% (Y. Thibeau, personal communication); Kretschmar and Scott (1976) reported an average value of 34.51 wt% and a range from 33.8 to 35.3 wt%.

The minimum detection limit for Au in pyrite from repeated analyses of the pyrite standard and many analyses of Au-poor arsenian pyrite was about 300 ppm (cf. Cabri et al. 1989; Cabri 1994, personal communication). We appreciated that the minimum detection limit for Au is markedly reduced at higher voltages and filament currents: Robinson and Graham (1992) reported values as low as 10 ppm for Au in sulfides at 40 kV, 470 nA, and count times of about 30 min. However, because of their fine grain size and susceptibility to beam damage, many of the materials presently analyzed were quite unsuited to these advanced techniques of analysis.

About 800 spot analyses of natural and synthetic ore minerals were made, although several hundred of these were reconnaissance in nature. Representative results for the synthetic phases are given in Table 1.

Grain fragments of selected experimental products were investigated by X-ray precession photography (Mo$K\alpha$, λ = 0.71069 Å). X-ray diffraction (XRD) powder patterns of FeS_2-AsS-S–composition material and other polycrystalline experimental products were obtained using a Gandolfi powder camera (Cr$K\alpha$, λ = 2.2909 Å).

TABLE 1. Extended.

Phase	FeS_2-AsS-S–composition material					
Expt	SA30	SA30	SA30	SA31	SA31	SA31
			wt%			
Fe	46.6	43.1	31.5	43.8	33.2	29.3
As	0.0	4.3	20.4	3.2	13.4	20.0
S	53.1	51.1	47.0	52.6	51.8	50.1
Au	0.0	0.0	0.0	0.0	0.13	0.10
Total	99.8	98.5	98.9	99.6	98.5	99.4
			at%			
Fe	33.5	31.8	24.5	31.7	24.7	22.2
As	0.0	2.4	11.8	1.7	7.4	11.3
S	66.5	65.8	63.7	66.3	67.1	66.0
Au	0.0	0.0	0.0	0.0	0.03	0.02
	Starting composition (at%; materials)					
Fe	20.5			19.0		
As	20.5			19.0		
S	59.0			62.0		
FeAs	X			X		
FeS						
Py						
As						
S	X			X		
As1						
	Experimental conditions					
T (°C)	215			215		
P (kbar)	1.4			1.4		
salt	NaCl			KCl		
t (d)	57			57		

EXPERIMENTAL RESULTS

Phases encountered in the present investigation of the Fe-As-S system at Au saturation included westerveldite, pyrrhotite, löllingite, arsenopyrite, arsenian pyrite and marcasite, pyrite, arsenic, realgar, orpiment, sulfur, and various other compositions or mixtures on the As-S join, and FeS_2-AsS-S–composition material. In experiments at 500 °C and below, crystal grains of native gold were not present (native gold was present only as physical contamination by capsule metal), and colloidal gold was not suspected during EMPA of sulfides and sulfarsenides. Small blebs of gold were commonly present in the products of the four experiments at 605 °C, confirming the observations of Clark (1960) on the corrosive effect of arsenian sulfide fluids on gold capsules.

Progress of reaction was very much dependent on the chemical combination of Fe, As, and S in the starting composition and on experimental temperature. Also, chemical communication within the charges was limited by the low proportion of fluid to solid and the lack of intimate mixing of starting materials. At and below 400 °C, starting FeS was invariably incompletely reacted with excess As and S, tending to be partly replaced and armored by arsenopyrite, marcasite, and pyrite. At 200–400 °C, starting pyrite reacted with excess As, and S was internally desiccated. At 300–400 °C, starting arsenopyrite alone showed no evidence of reaction with the fluid, either at grain boundaries or along fractures, and retained primary compositional zoning.

A starting mixture of FeAs + NaCl + H_2O yielded westerveldite + löllingite + iron oxide (or fayalite with added SiO_2) at 500–600 °C.

Arsenopyrite crystallized fairly readily by heterogeneous nucleation from mixtures of FeAs and excess As and S, but the products were very-fine grained and locally occurred as crystal masses. Crystallization of arsenopyrite from FeS and excess As was complex and temperature dependent, involving both replacement and heterogeneous nucleation. In general, progress of reaction varied markedly with communication in the gold capsule, with the least reaction (and uptake of Au) at the bottom of the charge and furthest away from the bulk of the fluid phase. Four texturally distinct types of arsenopyrite were generally present: topotaxial replacement product of pyrrhotite (starting FeS transformed into nonstoichiometric pyrrhotite); euhedral acicular grains forming a rim, overgrowth, or both to arsenopyrite 1; isolated or matted euhedral acicular grains, usually <10 μm in cross section (Fig. 2a; cf. Wu and Delbove 1989); and euhedral acicular grains (as arsenopyrite 2) forming a rim, overgrowth, or both to unreplaced pyrrhotite grains. Arsenopyrite 1 was the most common product, with replacement originating

at grain boundaries of massively aggregated pyrrhotite. The euhedral varieties of arsenopyrite preferentially developed from loosely aggregated starting materials or at locations with locally high fluid/solid ratios; e.g., matted crystals of arsenopyrite 3 developed in fluid pockets or veins within the pyrrhotite nutrients. Experiments at about 400 °C and of 1, 4, 14, and 57 d duration showed that all four textural varieties developed simultaneously. With increase in reaction and annealing time, arsenopyrite 1 became more pervasive and the heterogeneously nucleated varieties more euhedral. Also, compositional zoning present in the proto crystals did not homogenize with annealing.

Arsenian pyrite developed locally as a marginal alteration of starting pyrite and along cleavage traces of desiccated pyrrhotite in experiments at and above 300 °C. Marcasite was invariably arsenian and also locally developed with arsenopyrite, marginal to and within desiccated pyrite and as a narrow rim on pyrrhotite. It was identified petrographically and by the characteristic 110 line in powder XRD patterns of composite pyrite-marcasite intergrowths.

Material with a bulk composition field of FeS_2-AsS-S (Fig. 1), with many compositions falling in the more restricted field defined by the FeS_2-AsS and FeS_2-AsS_2 tie lines, was first observed in minor amounts in experiments at and above 300 °C. The proportion present increased with decreasing temperature, and in experiments conducted at about 200 °C, with the appropriate bulk composition and starting materials of either FeAs + S or pyrite + As + S, FeS_2-AsS-S–composition material was the major product phase. It occurred as compositionally zoned botryoidal masses and oscillatory-zoned oolitic bodies up to 100 μm in diameter (Figs. 2b and 2c). Individual zones were isotropic and homogeneous at the resolution of reflected-light microscopy and EMPA, and graded in width down to submicroscopic size. Optical reflectivity varied from high to low, for Fe-rich to Fe-poor compositions, respectively. However, Gandolfi XRD powder patterns of both homogeneous and zoned samples, some of which had been analyzed by EMPA and removed from polished sections, revealed only pure pyrite and orpiment, with trace marcasite and other As-S phases. Thus, the FeS_2-AsS-S–composition material was a composite of ultra-fine grains of phases of ideal end-member composition. It may have existed as a gel in the 200–300 °C experiments, as suggested by its desiccated appearance and porous core region (Figs. 2b and 2c), but this possibility was not investigated further. FeS_2-AsS-S–composition material appeared to be a quench phase in the higher temperature experiments.

A selection of EMPA compositions is given in Table 1, and compositions of arsenopyrite are plotted in Figures 3 and 4. With the notable exception of FeS_2-AsS-S–composition material, the phases present generally conformed to the known phase relations (Clark 1960; Kretschmar and Scott 1976). All sulfides and sulfarsenides, with the single exception of westerveldite, contained sporadic

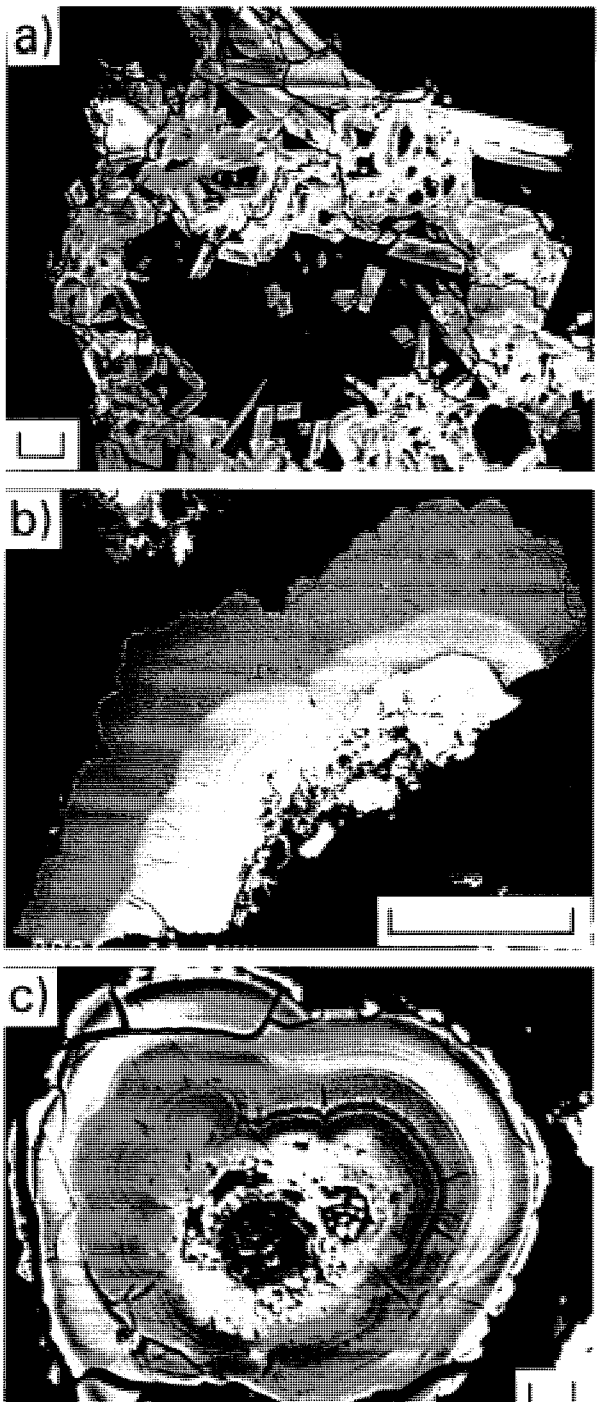

FIGURE 2. Backscattered electron images. (**a**) Matted euhedral acicular grains of arsenopyrite with zones of light, medium, and dark contrast; SA42 (400 °C, 57 d), scale bar is 10 μm. (**b**) Compositionally zoned botryoidal FeS_2-AsS-S–composition material; light contrast is As rich, dark contrast is FeS_2 rich; SA30 (215 °C, 57 d), scale bar is 100 μm. (**c**) Oscillatory-zoned oolitic FeS_2-AsS-S–composition material; SA29 (215 °C, 57 d), scale bar is 10 μm.

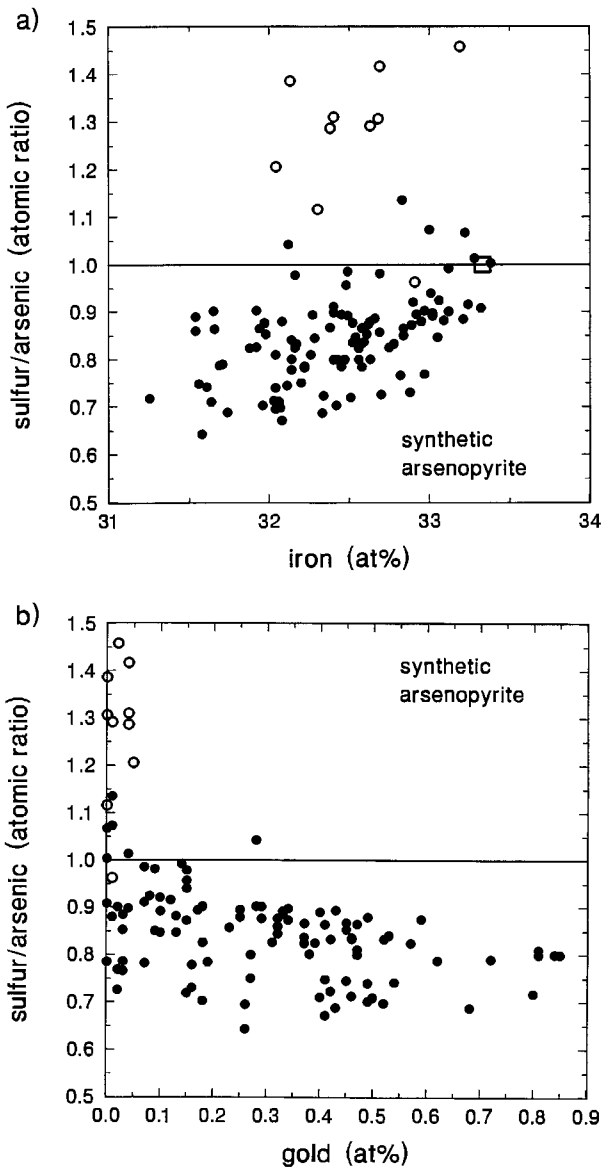

FIGURE 3. Compositions of synthetic arsenopyrite. The data are EMPA results for different growth zones of euhedral grains from five experiments. Solid circles are results for experiments with bulk compositions close to ideal FeAsS stoichiometry, SA13 (500 °C, 3 d), SA18 (415 °C, 14 d), SA41 (400 °C, 57 d), SA42 (400 °C, 57 d), and open circles are results for a bulk composition intermediate between FeAsS and FeS_2, SA43 (400 °C, 57 d). Note that almost all arsenopyrite compositions are Fe deficient (**a**), and high Au contents are restricted to As-excess arsenopyrite (**b**).

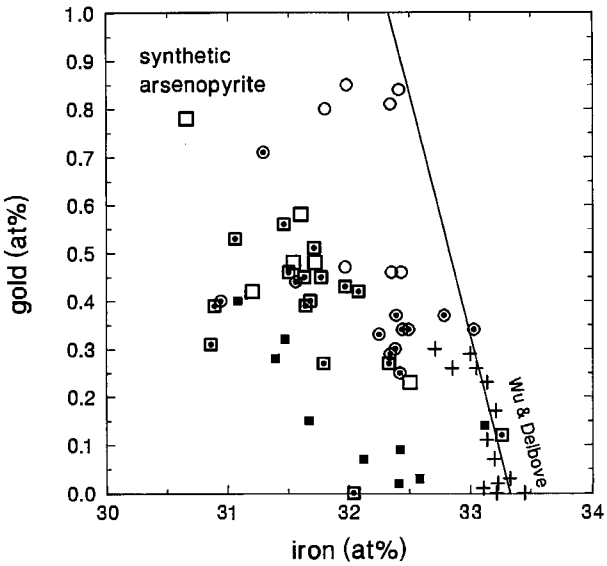

FIGURE 4. Variation of Au with Fe in euhedral grains of synthetic arsenopyrite. Open symbols are zones of light BSE contrast (cf. Fig. 2a), centered symbols are zones of medium contrast, and solid symbols are zones of dark contrast; squares are SA42 (400 °C, 57 d), circles are SA41 (400 °C, 57 d), crosses are data of Wu and Delbove (1989), line is substitution Fe = Au; all data are calculated to the formula $(Fe,Au,\square)As_{1\pm x}S_{1\pm x}$.

amounts of invisible gold. Westerveldite had a slightly metal-excess composition (Fe > As) and did not contain S when crystallized from ternary starting compositions. Similarly, Fe-rich pyrrhotite had only a trace amount of As, and S-rich pyrrhotite had no detectable As. The maximum S content observed in löllingite was 4.2 at%, and the maximum Au content of 0.25 wt% was significantly lower than that in arsenopyrite from the same experiment (0.94 wt%).

The two arsenopyrite analyses in Table 1 ($Fe_{32.7}As_{27.7}S_{39.2}$ and $Fe_{31.6}As_{41.5}S_{26.6}$) are representative of the composition range of our experimental products. The total variations in Fe (31.3–33.4), As (27.2–41.5), and S (26.6–39.6 at%) are somewhat greater than those reported for the dry Fe-As-S system (Kretschmar and Scott 1976) and nature (Klemm 1965; Kretschmar and Scott 1976; Sharp et al. 1985). Most of our synthetic arsenopyrite was deficient in Fe relative to the ideal FeAsS formula (Figs. 3a and 4). We observed the expected correlation of S/As ratio with bulk composition and temperature, but the inhomogeneity of our products did not permit precise thermometry over the small temperature interval investigated in detail (400–500 °C; cf. Kretschmar and Scott 1976). Also, arsenopyrite 1, the replacement product of pyrrhotite, contained significantly lower As and Au contents than the euhedral, heterogeneously nucleated arsenopyrite.

The Au contents of the synthetic arsenopyrite ranged up to 3.0 wt%, 0.85 at% (SA41, 400 °C, 57 d; Fig. 3b), a value far in excess of that reported for natural arsenopyrite (1.5 wt%; Johan et al. 1989) and synthetic arsenopyrite (1.7 wt%; Wu and Delbove 1989). The highest Au contents were in euhedral grains from experiments with a starting mixture of FeS + As in the proportion of ideal arsenopyrite (SA13, 500 °C, 3d; SA18, 415 °C, 14 d; and SA41 and SA42, 400 °C, 57 d). High Au contents correlated only with compositions that were As rich rel-

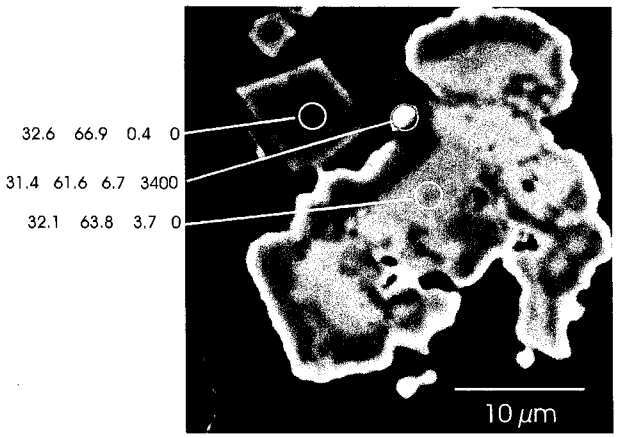

FIGURE 5. Digitally processed EMPA BSE image of composite pyrite grain from the Deep Star deposit, Carlin Trend, Nevada, showing As core, broad As-poor margin, and Au-bearing, Fe-deficient arsenian pyrite rim. Compositions are reported as atomic percent for Fe, S, and As, and parts per million for Au. Note the replacement relationships between compositional zones.

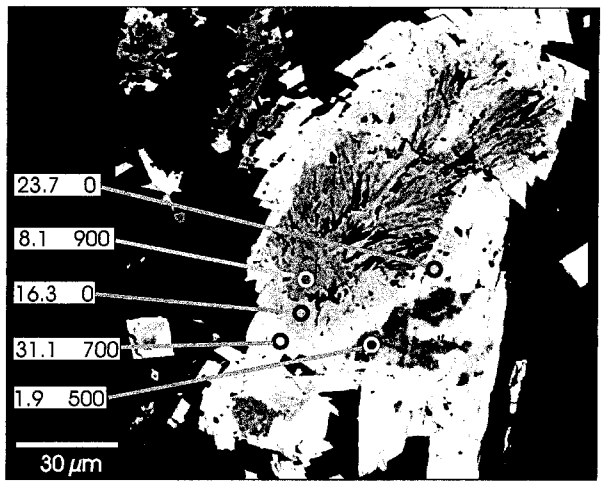

FIGURE 6. Digitally processed EMPA BSE image of composite, compositionally zoned arsenian-pyrite-marcasite-arsenopyrite grain from the Deep Star deposit, Carlin Trend, Nevada, showing arsenopyrite overgrowth. Compositions are reported as atomic percent for As and parts per million for Au.

ative to the ideal formula of FeAsS (Fig. 3b). Compositions showing excess S had only sporadic, low amounts of Au, which were generally lower than those reported below for coexisting arsenian pyrite and marcasite. The high Au contents are restricted to composition zones that are light (electron rich) in backscattered electron images (BSE; Fig. 2a). There is so much Au in these light zones that it largely accounts for the BSE contrast observed.

The As content of arsenian pyrite ranged up to 9.3 wt%, 5.0 at%. Au was detectable in about one-half of these spot analyses but generally was less than 0.1 wt%; the highest value recorded was 0.64 wt%. Arsenian marcasite was more As rich than the arsenian pyrite, with a maximum As content of 16.5 wt%, 9.7 at%. Au contents were again quite variable, and the maximum value was 0.35 wt%. The FeS_2-AsS-S–composition material was also gold bearing, in variable amounts ranging up to a maximum recorded value of 0.13 wt%.

DISCUSSION

Gold-sulfide association in Carlin Trend deposits

The present gold-sulfide ore samples from the Deep Star deposit consisted of structurally controlled breccia ore (Clode 1994; authors' work in progress). They contained up to about 30% of ultra-fine-grained pyrite and marcasite, which imparted a black sooty appearance to hand samples, and arsenopyrite, and up to 10% orpiment + realgar, and assayed between 1.17 and 5.04 ounces per ton of gold.

Pyrite was disseminated within fragments of host rocks, as vein filling and cement, and was predominately in the form of As- and Au-poor anhedral to euhedral grains. Ten to 25% of the pyrite was arsenian, which occurred variously as a replacement and overgrowth of As-poor pyrite (Fig. 5), as a replacement of Fe-bearing silicates and carbonates, as internal growth bands in composite pyrite grains [similar to the oscillatory-zoned grains described by Fleet et al. (1989, 1993) and Mumin et al. (1994)], in composite, compositionally zoned arsenian-pyrite-marcasite-arsenopyrite grains (Fig. 6), and as dispersed, heterogeneously nucleated and relatively homogeneous micrometer-size grains. Our observations on the common association of Au-rich arsenian pyrite overgrowths on As-poor pyrite (Fig. 5) were generally consistent with Arehart et al. (1993). However, the Au-bearing arsenian pyrite rims appeared to be in both replacement and overgrowth relationship with As-poor (Au-free) pyrite grains. The detailed micrograph (Fig. 5) reveals three generations of pyrite crystallization: an arsenian Au-free core region; an Au-poor pyrite that partly replaced the precursor pyrite and also crystallized by heterogeneous nucleation; and a narrow marginal overgrowth (or perhaps replacement) of Au-bearing arsenian pyrite. We also observed appreciably higher Au contents than Arehart et al. (1993) in some ore samples (up to 0.37 wt%).

No special precautions were taken to avoid physical contamination of ore minerals during preparation of polished sections. Smearing of soft ore minerals during mechanical polishing can introduce significant error into the quantitative determination of minor amounts of Au and Ag by EMPA (e.g., Remond et al. 1981, 1987). However, this type of interference would have been minimal in the present study. Native gold was not present in our ore samples from the Deep Star deposit and is relatively unimportant in Carlin Trend deposits in general (e.g., Bakken et al. 1989, 1991). Gold filings from capsule material were present in some polished sections of experimental products but only in minor amounts.

Marcasite was relatively abundant, occurring as an in-

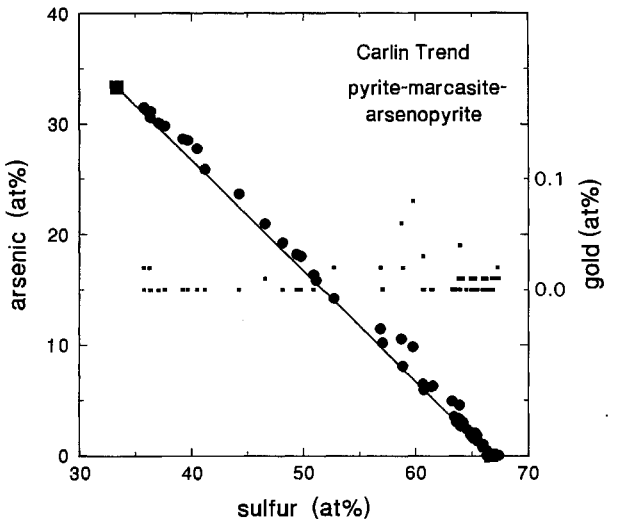

FIGURE 7. Compositions of arsenian pyrite and marcasite and arsenopyrite from Carlin Trend ores. Circles are As content and small squares are Au content. Note the continuity of EMPA compositions from FeS_2 to FeAsS. Also, almost all compositions are Fe deficient, with As contents plotting above the FeS_2-FeAsS line. Figure includes data for compositionally zoned arsenian-pyrite-marcasite-arsenopyrite grains but not the results for sample DS17 of Figure 8.

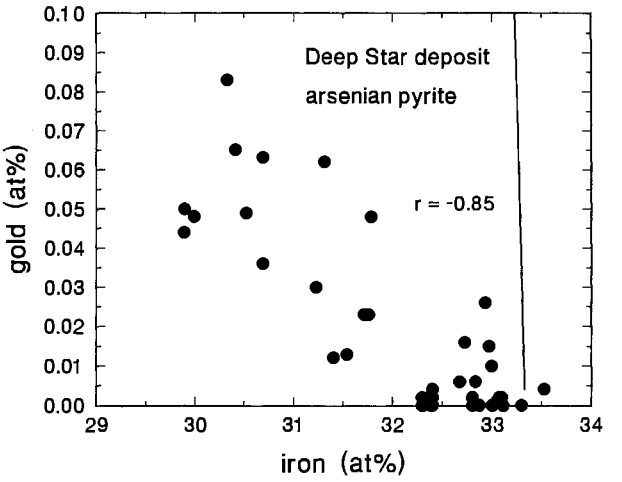

FIGURE 8. Inverse correlation of Au and Fe in arsenian pyrite and marcasite from the Deep Star deposit. Line is substitution Fe = Au (sample DS17).

tergrowth with both As-poor and arsenian pyrite. Arsenopyrite was also abundant as isolated euhedral grains and overgrowths to pyrite and, less commonly, overgrowths and internal zones of the composite, compositionally zoned arsenian-pyrite-marcasite-arsenopyrite intergrowths (Fig. 6).

The compositions of pyrite, arsenian pyrite and marcasite, and arsenopyrite from the Carlin Trend gold deposits extended from FeS_2 to near FeAsS (Fig. 7). The range in As content of arsenian pyrite exceeded that reported for pyrite from other gold deposits (Fleet et al. 1989) and the present experiments. The arsenian pyrite was also markedly Fe deficient and generally had elevated amounts of Au (Fig. 8). On the other hand, the arsenopyrite was restricted to compositions more S rich than the ideal stoichiometry, consistent with low-temperature crystallization (cf. Kretschmar and Scott 1976), and was relatively Au poor (Fig. 7), consistent with the present observations for synthetic S-rich arsenopyrite. The compositions intermediate between arsenian pyrite and arsenopyrite (about 57–40 at% S; Fig. 7) were all from relatively broad and seemingly homogeneous interior zones of the composite, compositionally zoned arsenian-pyrite-marcasite-arsenopyrite intergrowths (Fig. 6). However, these interior zones were still too narrow for meaningful XRD analysis with conventional X-ray sources, and, therefore, the possibility that the intermediate compositions represent two-phase mixtures has not been excluded.

Synthetic arsenopyrite and arsenian pyrite and marcasite

Crystallization of pyrite, marcasite, and arsenopyrite is well known to be sluggish and reaction-path dependent at low temperature (e.g., Murowchick and Barnes 1986; Schoonen and Barnes 1991; Wu and Delbove 1989). Previous and present studies on natural assemblages have revealed widespread metastable persistence of solid solutions along the FeS_2-FeAsS join (Fig. 7; also, Fig. 9 of Fleet et al. 1989). Kretschmar and Scott (1976) were forced to accept that most of the characteristic compositional zoning in natural arsenopyrite is a nonequilibrium feature reflecting the kinetics of mineral growth and local fluctuations in the activity ratio of S to As species. Therefore, we did not set out in the present experimental investigation to establish the stable phase relations in the Fe-As-S system at low temperature, anticipating experimental difficulties and suspecting that such stable phase relations may have little relevance to the natural gold-sulfide ore assemblages. Clearly, had the experiments been reversed, the product phases likely would have corresponded to those of the dry system investigated at higher temperature by Clark (1960) and Kretschmar and Scott (1976).

Thus, we merely attempted to reproduce the natural assemblages and phase compositions of Au-bearing Fe-As-S minerals. The experiments were designed to limit chemical communication within the charges and to promote surface-controlled and topotaxial replacement reactions. We used a low fluid/solid ratio, the starting materials were not ground and mixed, and the experiments were not interrupted for further grinding and mixing to promote homogenization of the product phases.

The present results for the euhedral arsenopyrite crystals (acicular morphology, compositional zonation, wide variation in S/As ratio and in Au content within single

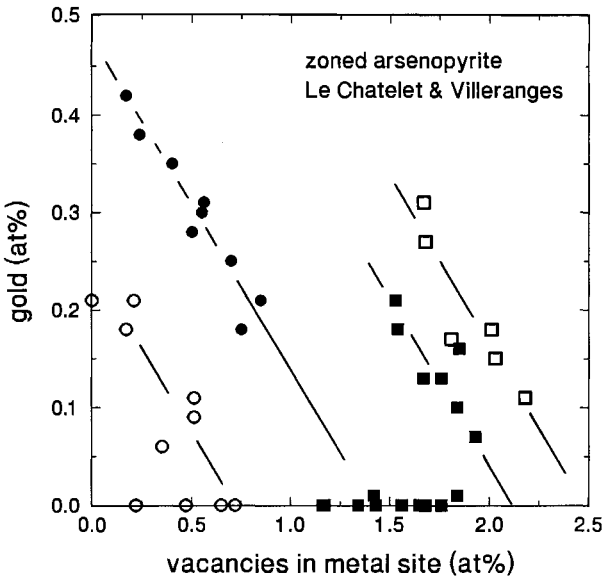

FIGURE 9. Composition of arsenopyrite from the Châtelet and Villeranges gold deposits, Central Massif, France. Squares are Le Châtelet, solid for growth zone A and open for growth zone B; circles are Villeranges, solid for growth zone C and open for growth zone D. Data are from Johan et al. (1989) recalculated to the formula $(Fe,Au,\square)(As,Sb)_{1\pm x}S_{1\pm x}$; lines were visually fitted.

grains and from one zone to another, deficiency in Fe) are comparable to those of Wu and Delbove (1989), who experimented at 500 °C using a starting mixture of Fe_2O_3 + As + S and an appreciably higher fluid/solid ratio. Our compositionally zoned euhedral arsenopyrite broadly reproduced arsenopyrite from gold deposits as well, although the Au contents and variation in composition are higher than commonly observed in nature.

Arsenian pyrite and marcasite formed readily at 300–400 °C, but only in limited amounts and, apparently, only by replacement of pyrite and pyrrhotite. We previously observed Au-bearing arsenian pyrite as a replacement product of preexisting pure pyrite from an epithermal gold deposit, where the paragenetic sequence was confirmed by the fracture-controlled spatial distribution of the arsenian pyrite (Fleet and Chryssoulis, unpublished results). Also, the Au-bearing arsenian rims of fine-scale pyrite from the Deep Star deposit, Carlin Trend, appear to be partly replacement in nature. However, arsenian pyrite elsewhere (e.g., Fleet et al. 1989) generally appears to have formed by crystal growth. To this extent, we have not reproduced the complex pyrite microstructures reported by Fleet et al. (1989, 1993) but, perhaps, would not have expected to do so without having some mechanism in the experimental procedure that simulated episodic fluctuation in fluid composition. The colloform textures and oscillatory zonation that characterize some natural arsenian pyrite is reproduced by the FeS_2-AsS-S–composition material, albeit for more As- and S-rich compositions than in nature, and these growth textures are very similar to colloform pyrite of other paragenesis. Both reaction kinetics and solution conditions must exert considerable influence on the precipitation of phases, like pyrite, that nucleate with difficulty. Clearly, it is not possible to simulate the natural conditions (time scale, variation in fluid conditions, etc.) precisely in the laboratory.

The present experiments have reproduced the full range of S/As ratio for arsenian pyrite reported by Fleet et al. (1989). However, we have not reproduced the virtual continuum of FeS_2-FeAsS compositions presently reported for the zonal grains from the Deep Star deposit consisting of pyrite, arsenian pyrite, marcasite, and arsenopyrite (Fig. 7).

Uptake of As and Au by sulfide minerals

Arsenian pyrite and arsenopyrite are both important hosts for invisible gold in nature and in laboratory synthesis. Significant amounts of invisible gold in pyrite and marcasite correlate only with As-rich compositions and in arsenopyrite only with As-excess compositions (Fleet et al. 1993; present Fig. 3b; Wu and Delbove 1989). Also, arsenopyrite, and particularly Au-bearing arsenopyrite, tends to be Fe deficient in nature (e.g., Klemm 1965; Kretschmar and Scott 1976; Sharp et al. 1985; present Fig. 7) and in laboratory synthesis (Wu and Delbove 1989; Fig. 3a), as does Au-bearing arsenian pyrite and marcasite (Fig. 8; Table 1). Thus, invisible gold in sulfide minerals is associated with both anomalous As content and Fe deficiency. The structural accommodation of the metal deficiency, the oxidation state of cations and ligand atoms, and the physical and chemical state of Au are all important and troublesome questions in the crystal chemistry of chalcogenides (compounds of metals with S, Se, and Te) and pnictides (compounds of metals with P, As, Sb, and Bi) and the geochemistry of Au.

Hypothetically, Fe deficiency in arsenian pyrite and marcasite and arsenopyrite could be accommodated by either nonstoichiometry or cationic As. Nonstoichiometry is very extensive in transition-metal chalcogenides belonging to the NiAs-CdI_2 structure series (e.g., Jeannin 1970; and pyrrhotite). Therefore, it does not seem unreasonable to expect nonstoichiometry in pyrite and marcasite as well, particularly where the chalcogen ligand (S, Se, Te) is partially substituted by a pnictogen (P, As, Sb, Bi) and in light of the wealth of recent EMPA data for arsenian pyrite and marcasite and arsenopyrite.

Johan et al. (1989) reported some remarkable element correlations for individual Au-rich growth zones of arsenopyrite from the Châtelet and Villeranges deposits, Massif Central, France, which they interpreted by invoking complex solid solutions of the type $(Fe,Au,As,Sb)As_{1\pm x}S_{1\pm x}$, and a substitution mechanism of 2As = Au (or Sb) + Fe. Although As is formally more electropositive than Au (electronegativities are 1.8–1.9 for Fe, 2.1 for As, 2.3 for Au, and 2.6 for S; Batsanov 1968) and As^{3+} is similar in size to Fe^{3+} (effective ionic radii for octahedral coordination are 0.58 and 0.65 Å, respectively; Shannon 1976), the octahedral cation site of arsenopyrite

seems quite unsuited to cationic As, which prefers a pyramidal coordination with S (e.g., AsS_3, $AsAsS_2$, etc.). Also, cationic As in arsenopyrite would result in As^{3+}-As^{2-} bonds, which seem energetically unfavorable. Bond resonance, which is often invoked to explain the valence matching required for As-As interactions in sulfarsenide compounds, would significantly modify the crystal-chemical properties of the cationic arsenic species. Moreover, Sb and Au in the Châtelet and Villeranges arsenopyrite are essentially mutually exclusive in a manner analogous to As and Ag in tetrahedrite (e.g., Fig. 8 of Mumin et al. 1994). The EMPA results of Johan et al. (1989) are presently recalculated to a nonstoichiometric formula [$(Fe,Au,\square)(As,Sb)_{1\pm x}S_{1\pm x}$, where $\square$ is a cation vacancy], yielding element correlations that indicate a substitution mechanism of the type $2Fe + Au = 3\square$ (Fig. 9).

The high Au contents of the Châtelet arsenopyrite are restricted to As-excess compositions: The EMPA locations for growth zone A (Fig. 9) that have no observable Au all have compositions with S/As > 1.0. However, growth zone D of the Villeranges arsenopyrite does have Au-rich compositions with S/As > 1.0, although the overall correlation of increasing Au with increasing As is maintained.

Consideration of the oxidation state of the cations and ligand atoms in arsenian pyrite and marcasite and arsenopyrite is beyond the scope of the present paper, requiring new theoretical calculations and chemical spectroscopic measurements (e.g., microbeam XPS) to study the fine-scale arsenian-pyrite-marcasite-arsenopyrite intergrowths effectively. Superficially, it does appear that the covalently bonded sulfarsenide atom pairs have a remarkable capacity for controlling oxidation state in pyrite-marcasite-arsenopyrite materials.

In respect to the physical state of invisible gold in arsenian pyrite and marcasite and arsenopyrite, there is little direct evidence favoring colloidal gold to the exclusion of lattice-bound Au (cf. Bakken et al. 1989, 1991). In the absence of the routine observation of nanometer-scale, evenly dispersed gold particles, the present element correlations are quite compelling evidence favoring lattice-bound Au. Invisible gold correlates with As content in both natural and synthetic arsenian pyrite and marcasite and, in high amounts, with excess As in most natural and all synthetic arsenopyrite (e.g., Fleet et al. 1993; present Figs. 3b, 7, and 9; present Table 1), and with Fe deficiency in natural and synthetic arsenian pyrite and marcasite and arsenopyrite (present Figs. 7–9; present Table 1; Johan et al. 1989). Also, the light (Au-rich) zones in the BSE images of the present synthetic arsenopyrite (Fig. 2a) have fairly uniform contrast, indicating an even spatial distribution of the heavy Au atoms. These consistent observations are incompatible with the incorporation of invisible gold as nanometer-scale particles during crystal growth. It is possible that very small (ångstrom-scale) clusters of Au atoms, perhaps stabilized in the ore fluid as cluster compounds (e.g., Hall and Mingos 1984), could be attracted to the growth surfaces of sulfides by surface charge resulting from the local As-rich, Fe-deficient sites or excited surface states or deposited by sorption and reduction (e.g., Mycroft et al. 1995). However, such small clusters would surely be revealed routinely as defects in high-resolution TEM images of auriferous arsenian pyrite and marcasite and arsenopyrite (cf. Bakken et al. 1991).

We had anticipated that the element correlations for the natural and synthetic arsenian pyrite and marcasite and arsenopyrite would reveal the oxidation state of the invisible gold (i.e., Au^0, Au^{1+}, etc.). Unfortunately, although the amount of invisible gold is generally always less than the excess of As or the deficiency of Fe (Figs. 3, 4, and 7–9), consistent linear trends are not evident. We note that the correspondence of the Wu and Delbove (1989) results for synthetic arsenopyrite with the Fe = Au substitution line (cf. Fig. 4) may be an artifact of the limited data presented in this earlier study.

The EMPA results of Johan et al. (1989) for the Châtelet and Villeranges arsenopyrite suggest a closer approach to local equilibration for individual growth zones than the present experimental products. The four growth zones analyzed (Fig. 9) each reveal the same substitution mechanism $2Fe + Au = 3\square$, but this is not helpful in assigning the oxidation state of Au. The Châtelet and Villeranges arsenopyrite samples, in fact, show an increase in invisible gold with decreasing metal-site vacancies, which is the opposite of the trends for arsenian pyrite and marcasite from Carlin Trend and synthetic arsenian pyrite and marcasite and arsenopyrite.

We suggest that in sediment-hosted gold-deposit systems, Au is removed from ore fluids largely by chemisorption on the As-rich, Fe-deficient growth surfaces of pyrite, marcasite, and arsenopyrite. The active sites fixing Au would be formed by soft Lewis bases (e.g., As_2, AsS), and vacancies in nearest-neighbor cation sites would permit the Au atoms to customize their local atomic environment. Thus, the solid solution of Au could be accompanied by point defects, and its nearest-neighbor coordination in the bulk sulfides need not necessarily be octahedral. However, we note that Cu, a metal with a somewhat similar coordination chemistry to Au, does form a pyrite-structure phase at high pressure (King and Prewitt 1979). We emphasize that the hypothesized chemisorption process is not restricted to crystal growth. The presence of arsenian pyrite and marcasite as replacement phases in both natural and laboratory products suggests that in these cases the hypothesized chemisorption must also be accompanied by coupled replacement by As, Au, and vacancies.

The chemisorbing surface would be conditioned differently for different solution conditions, establishing only a local equilibrium with the Au-bearing fluid. Thus, the incorporation of invisible gold would be intrinsically nonsystematic in terms of crystal-chemical parameters, depending only on the solution conditions imparting a minimum excess of As and deficiency of Fe to the active surface. This type of control on the chemisorption process, coupled with the tendency of the covalently bonded

As-S interactions to act as an oxidation-state buffer, readily accounts for the lack of systematic linear atomic substitution trends. Thus, we conclude that invisible gold in arsenian pyrite and marcasite and arsenopyrite represents Au removed from ore fluids by chemisorption at As-rich, Fe-deficient surface sites and incorporated in the solids in metastable solid solution. It follows that the metastable crystallization of FeS_2-FeAsS solid solutions (Fig. 7) reflects a control by surface-chemical processes also.

This study is another step in the understanding of the distribution, chemical state, and manner of incorporation of invisible gold into arsenian pyrite and marcasite and arsenopyrite. Previous studies have documented the common occurrence of oscillatory-zoned auriferous arsenian pyrite in sediment-hosted gold deposits, shown that the anomalous As content is held in metastable solid solution, and demonstrated that the invisible gold is spatially associated with local enrichment in As (e.g., Fleet et al. 1989, 1993; Bakken et al. 1991; Mumin et al. 1994). We have demonstrated that invisible gold correlates strongly with As enrichment and Fe deficiency in both pyrite-marcasite and arsenopyrite. This correlation favors a chemisorption process for the incorporation of Au into these minerals and makes dominant control by entrapment of colloidal gold less likely. However, HRTEM studies are required to establish that colloidal gold particles less than 20–50 Å in size do not quantitatively account for the invisible gold fraction of auriferous pyrite.

The oxidation state of the proposed lattice-bound invisible gold remains uncertain. Indeed, experimental determination of the precise chemical state of trace amounts of Au in pyrite and marcasite may continue to be very difficult. Therefore, meaningful future studies may be restricted to As-rich growth zones of arsenopyrite, which have Au contents of up to 3.0 wt%.

Finally, we have not shown that Fe deficiency is an essential requirement for the chemisorption of Au onto growth surfaces of arsenian pyrite and marcasite and arsenopyrite. We report only that Au content correlates with Fe deficiency and thus suggest that active growth surfaces are both As rich and Fe deficient.

Acknowledgments

We thank Y. Thibeau and Shao Yue for assistance with EMPA; G.B. Arehart, Z. Johan, B.M. Bakken, an unnamed referee, and D.W. Mogk for helpful reviews of earlier versions of the manuscript; Newmont Gold Company, Carlin, for provision of samples and geological information on the Deep Star mine and other gold deposits along the Carlin Trend; and the Natural Sciences and Engineering Research Council of Canada for financial support.

References cited

Arehart, G.B., Chryssoulis, S.L., and Kesler, S.E. (1993) Gold and arsenic in iron sulfides from sediment-hosted disseminated gold deposits: Implications for depositional processes. Economic Geology, 88, 171–185.

Bakken, B.M., Hochella, M.F., Jr., Marshall, A.F., and Turner A.M. (1989) High-resolution microscopy of gold in unoxidized ore from the Carlin mine, Nevada. Economic Geology, 84, 171–179.

Bakken, B.M., Fleming, R.H., and Hochella, M.F., Jr. (1991) High-resolution microscopy of auriferous pyrite from the Post deposit, Carlin district, Nevada. In D.M. Hausen, W. Petruk, R.D. Hagni, and A. Vassiliou, Eds., Process Mineralogy XI: Characterization of metallurgical and recyclable products, p. 13–23. The Minerals, Metals, and Materials Society, Warrendale, Pennsylvania.

Batsanov, S.S. (1968) The concept of electronegativity. Conclusions and prospects. Russian Chemical Reviews, 37, 332–351.

Berger, B.R., and Bagby, W.C. (1991) The geology and origin of Carlin-type gold deposits. In R.P. Foster, Ed., Gold metallogeny and exploration, p. 210–248. Blackie, Glasgow.

Cabri, L.J., Chryssoulis, S.L., De Villiers, J.P.R., LaFlamme, J.H.G., and Buseck, P.R. (1989) The nature of "invisible" gold in arsenopyrite. Canadian Mineralogist, 27, 353–362.

Cathelineau, M., Boiron, M.-C., Holliger, P., Marion, P., and Denis, M. (1989) Gold in arsenopyrites: Crystal chemistry, location and state, physical and chemical conditions. Economic Geology Monograph 6, 328–341.

Christensen, O.D. (1993) Carlin trend geological overview. In O.D. Christensen, Ed., Gold deposits of the Carlin Trend, Nevada, p. 12–26. Society of Economic Geologists Guidebook Series 18, Denver.

Clark, L.A. (1960) The Fe-As-S system: Phase relations and applications. Economic Geology, 55, 1345–1381.

Clode, C.H. (1994) Geology of the Deep Star gold deposit, Eureka County, Nevada. Northeastern Nevada Section of A.I.M.E. Spring Field Trip. Abstract Volume.

Cook, N.J., and Chryssoulis, S.L. (1990) Concentrations of "invisible" gold in the common sulfides. Canadian Mineralogist, 28, 1–16.

Fleet, M.E., MacLean, P.J., and Barbier, J. (1989) Oscillatory-zoned As-bearing pyrite from strata-bound and stratiform gold deposits: An indicator of ore fluid evolution. Economic Geology Monograph 6, 356–362.

Fleet, M.E., Chryssoulis, S.L., MacLean, P.J., Davidson, R., and Weisener, C.G. (1993) Arsenian pyrite fom gold deposits: Au and As distribution investigated by SIMS and EMP, and color staining and surface oxidation by XPS and LIMS. Canadian Mineralogist, 31, 1–17.

Hall, K.P., and Mingos, D.M.P. (1984) Homo- and heteronuclear cluster compounds of gold. In S.J. Lippard, Ed., Progress in inorganic chemistry, vol. 32, p. 237–325. Wiley, New York.

Jeannin, Y.P. (1970) Recent progress in the investigation of nonstoichiometry. In A. Rabenau, Ed., Problems of nonstoichiometry, p. 77–129. North-Holland, Amsterdam.

Johan, Z., Marcoux, E., and Bonnemaison, M. (1989) Arsénopyrite aurifère: Mode de substitution de Au dans la structure de FeAsS. Academie de Sciences (Paris) Comptes Rendus, 308, 185–191.

King, H.E., Jr., and Prewitt, C.T. (1979) Structure and symmetry of CuS_2 (pyrite structure). American Mineralogist, 64, 1265–1271.

Klemm, D.D. (1965) Synthesen und Analysen in den Dreiecksdiagrammen FeAsS-CoAsS-NiAsS und FeS_2-CoS_2-NiS_2. Neues Jahrbuch für Mineralogie Abhandlungen, 103, 205–255.

Kretschmar, U., and Scott, S.D. (1976) Phase relations involving arsenopyrite in the system Fe-As-S and their application. Canadian Mineralogist, 14, 364–386.

Kuranti, G. (1941) Synthetic study of gold-containing pyrite. Chemical Abstracts, 35, 3563.

MacLean, P.J. (1991) The characterization of pyrite from gold deposits. Ph.D. thesis, University of Western Ontario, London, Ontario, Canada.

MacLean, P.J., and Fleet, M.E. (1989) Detrital pyrite in the Witwatersrand gold fields of South Africa: Evidence from truncated growth banding. Economic Geology, 84, 2008–2011.

Mao, Shui He (1991) Occurrence and distribution of invisible gold in a Carlin-type gold deposit in China. American Mineralogist, 76, 1964–1972.

Michel, D., Giuliani, G., Olivo, G.R., and Marini, O.J. (1994) As growth banding and the presence of Au in pyrites from the Santa Rita gold vein deposit hosted in Proterozoic metasediments Goiás State, Brazil. Economic Geology, 89, 193–200.

Mumin, A.H., Fleet, M.E., and Chryssoulis, S.L. (1994) Gold mineralization in As-rich mesothermal gold ores of the Bogosu-Prestea mining district of the Ashanti Gold Belt, Ghana: Remobilization of "invisible" gold. Mineralium Deposita, 29, 445–460.

Murowchick, J.B., and Barnes, H.L. (1986) Marcasite precipitation from

hydrothermal solutions. Geochimica et Cosmochimica Acta, 50, 2615–2630.

Mycroft, J.R., Bancroft, G.M., McIntyre, N.S., and Lorimer, J.W. (1995) Spontaneous deposition of gold on pyrite from solutions containing Au(III) and Au(I) chlorides: Part I. A surface study. Geochimica et Cosmochimica Acta, 59, 3351–3365.

Radtke, A.S. (1985) Geology of the Carlin gold deposit, Nevada, 124 p. U.S. Geological Survey Professional Paper 1267.

Remond G., Holloway, P.H., and Le Gressus, C. (1981) Electron spectroscopy and microscopy for studying surface changes of mechanically prepared pyrite and quartz. Scanning Electron Microscopy, 1, 483–492.

Remond G., Cesbron, F., Traxel, K., Campbell, J.L., and Cabri, L.J. (1987) Electron microprobe analysis and proton induced X-ray spectrometry applied to trace element analysis in sulfides: Problems and prospects. Scanning Microscopy, 1, 1017–1037.

Robinson, B.W., and Graham, J. (1992) Advances in electron microprobe trace-element analysis. Journal of Computer-Assisted Microscopy, 4, 263–265.

Rota, J.C. (1993) Geology and related studies at the Gold Quarry deposit, Nevada. In O.D. Christensen, Ed., Gold deposits of the Carlin Trend, Nevada, p. 67–78. Society of Economic Geologists Guidebook Series 18, Denver.

Schoonen, M.A.A., and Barnes, H.L. (1991) Mechanisms forming pyrite and marcasite from solution: III. Hydrothermal processes. Geochimica et Cosmochimica Acta, 55, 3491–3504.

Shannon, R.D. (1976) Revised effective ionic radii and systematic studies of interatomic distances in halides and chalcogenides. Acta Crystallographica, A32, 751–767.

Sharp, Z.D., Essene, E.J., and Kelly, W.C. (1985) A re-examination of the arsenopyrite geothermometer: Pressure considerations and applications to natural assemblages. Canadian Mineralogist, 23, 517–534.

Tossel, J.A., Vaughan, D.J., and Burdett, J.K. (1981) Pyrite, marcasite, and arsenopyrite type minerals: Crystal chemical and structural principles. Physics and Chemistry of Minerals, 7, 177–184.

Wagner, F.E., Sawicki, J.A., Friedl, J., Mandarino, J.A., Harris, D.C., and Cabri, L.J. (1994) ^{197}Au Mössbauer study of the gold-silver ditellurides sylvanite, krennerite and calaverite. Canadian Mineralogist, 32, 189–201.

Wells, J.D., and Mullens, T.E. (1973) Gold-bearing arsenian pyrite determined by microprobe analysis, Cortez and Carlin gold mines, Nevada. Economic Geology, 68, 187–201.

Wijeyesekera, S.D., and Hoffmann, R. (1983) Marcasites and arsenopyrites: Structure, bonding, and electrical properties. Inorganic Chemistry, 22, 3287–3300.

Wu, X., and Delbove, F. (1989) Hydrothermal synthesis of gold-bearing arsenopyrite. Economic Geology, 84, 2029–2032.

Manuscript received March 5, 1996
Manuscript accepted September 17, 1996